Chapter-2

Design and Development of Extremely Low-frequency Pulsed Electromagnetotherapy Chamber for *In Vivo* and *In Vitro* Studies

2.1 Introduction

Bioelectromagnetics is a non-invasive technique providing an alternative therapeutic methodology for numerous biomedical applications. It utilizes ELF-MFs to treat soft and hard tissue diseases (Shupak et al., 2003). The Helmholtz, Merritt, and Ruben coil arrangements are the most popular design configurations for uniform magnetic field generation systems (Modi et al., 2016). However, various bioelectromagnetic studies indicated that the Helmholtz configuration is the most straightforward to implement (Rubik, 2002; Shupak et al., 2003; Vallbona and Richards, 1999). Although the Helmholtz coil's underlying theory is reasonably well understood, designing a monoaxial coil primarily depends upon the intended applications. Furthermore, magnetic field strength and uniformity within a given volume, response time, and the coil's inductance can vary significantly depending on the applications.

The design, implementation, and validation of a homogenous alternating MF are represented in the upcoming sections in this chapter. Its primary applications are observing MF exposure effects *in vivo* and *in vitro*. The materials and methods sections discuss the proposed systems' requirements. The objective is to design and fabricate an 50 Hz ELF-PEMF device capable of generating a uniform MF in host cells and tissues under *in vitro* and *in vivo* conditions.

2.2 Material and methods

2.2.1 Design considerations

We selected a circular coil configuration rather than a square one due to its simplicity in design, fabrication, assembly, and cost-effectiveness (Kohli et al., 2022). The MF must be homogenous with negligible variation, regardless of location within the limited volume. Moreover, the MF must

accommodate the animal cage and incubator chamber to confirm adequate exposure under *in vivo* and *in vitro* conditions.

2.2.2 Mathematical modeling

In a custom-made device, it is necessary to determine the MF close to the coil's center. According to the Biot-Savart law, the magnetic field depends on the current, number of wire turns, coil size, and separation distance between coil pair (Alvarez et al., 2012a; Caparelli and Tomasi, 2001; Restrepo-álvarez et al., 2017). The Biot-Savart law can be expressed as

$$dB = \frac{\mu_0}{4\pi}\left(\frac{I * dl * \sin(\theta)}{r^2}\right) \qquad (2.1)$$

Here,

$I = \text{Current flow inside coils in Columb per sec or ampere (A)} (M^0L^0T^0A^1)$

$dl = \text{Vector line segment in meter } (M^0L^1T^0)$

$r = \text{Radial distance between dl and point P in meter } (M^0L^1T^0)$

Now as shown in figure 2.1(A),

$$dB = \frac{\mu_{0*I}}{4\pi}\left(\frac{\cos\Phi}{d}\right)d\Phi \qquad (2.2)$$

Hence, the magnetic field due to the whole conductor

$$B = \int dB \qquad (2.3)$$

$$B = \frac{\mu_0}{2\pi}\left(\frac{I}{d}\right) \qquad (2.4)$$

Equation (2.4) gives the value of magnetic flux density (B) at point (P) due to the conductor of infinite length, and for an infinitely long conductor, $\alpha = \beta = \frac{\pi}{2}$ as shown in figure 2.1(B).

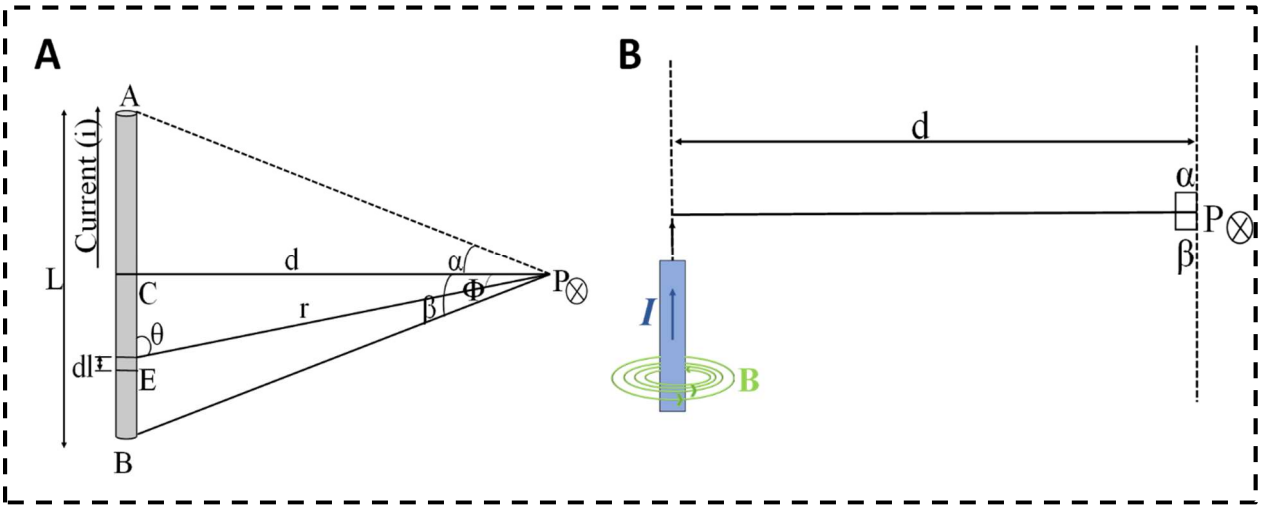

Figure 2.1 Biot-Savart law. (A) Magnetic field generation at point "P" along section (dl) at radial distance (r), (B) The representation of the magnetic field orientation along wire length.

The magnetic field at the center of the co-axial coil can be represented by integrating equation (2.1)

$$B = \frac{\mu_0 I}{4\pi r^2} \int_0^{2\pi r} dl \qquad (2.5)$$

since $\theta = 90^{\circ}$

$$B = \frac{\mu_0}{2r} (N * I) \qquad (2.6)$$

2.2.3 Helmholtz coil equation

The Helmholtz coils are widely used for experimental purposes where MF uniformity is crucial, and equation (2.7) explains the exact value of the MF at the center of coils (Alvarez et al., 2012b; Restrepo-álvarez et al., 2017). The magnetic flux density (B) at the midpoint between the coils can

be represented by the following expression

$$B = \left(\frac{4}{5}\right)^{3/2} \left(\frac{I*N*\mu}{R_c}\right) \qquad (2.7)$$

Here,

$B =$ Magnetic flux density in Tesla $(M^1L^0T^{-2}A^{-1})$

$N =$ Number of wire turns

$R_c =$ Coil radius (meter) $(M^0L^1T^0)$

$I =$ Current through coils (Ampere) $(M^0T^0L^0A^1)$

and

$\mu =$ Permeability of free space $(4\pi \text{ x } 10^{-7} \text{ H/m})(M^1L^1T^{-2}A^{-2})$

2.2.4 Optimum distance between coils

According to the Helmholtz configuration, co-axial circular coils must be arranged symmetrically, one on each side of the experimental area separated by a distance ($r = 0.265$ m) equal to the radius of the coils as shown in the following expression.

$$r = R_c \qquad (2.8)$$

Each coil must carry an equal amount of current in the same direction to reduce the non-uniformity of the field at the coils' centers, and magnetic flux density (B) gets affected by increasing the coil separation distance (r) (Grant and Phillips, 2013; Jones, 2013; Ramsden, 2011).

2.2.5 Helmholtz coil configuration

The magnetic flux density shown by equation (2.7) is proportional to wire turns (N) and supplied current (I) but inversely proportional to the coil radius (R_c). Therefore, any changes in the structural aspects will be implicated in selecting structural and electrical aspects like the number of wires turn, wire length, and uniformity within the cubic sections.

2.2.5.1 Structural design

According to the literature, the monoaxial coil system must generate a homogenous MF for bioelectromagnetic studies. Based on the design considerations, mathematical modelling, Helmholtz equation and optimum distance between coils, we finalized the coil configuration which includes inner/outer coil diameter as per the requirement of minimum area ($30 \times 35.5\ \mathrm{cm}^2$) between the coils with minimum field variation. Figure 2.2 (A-B) shows the coil configuration and MF direction due to the current flow inside coils respectively.

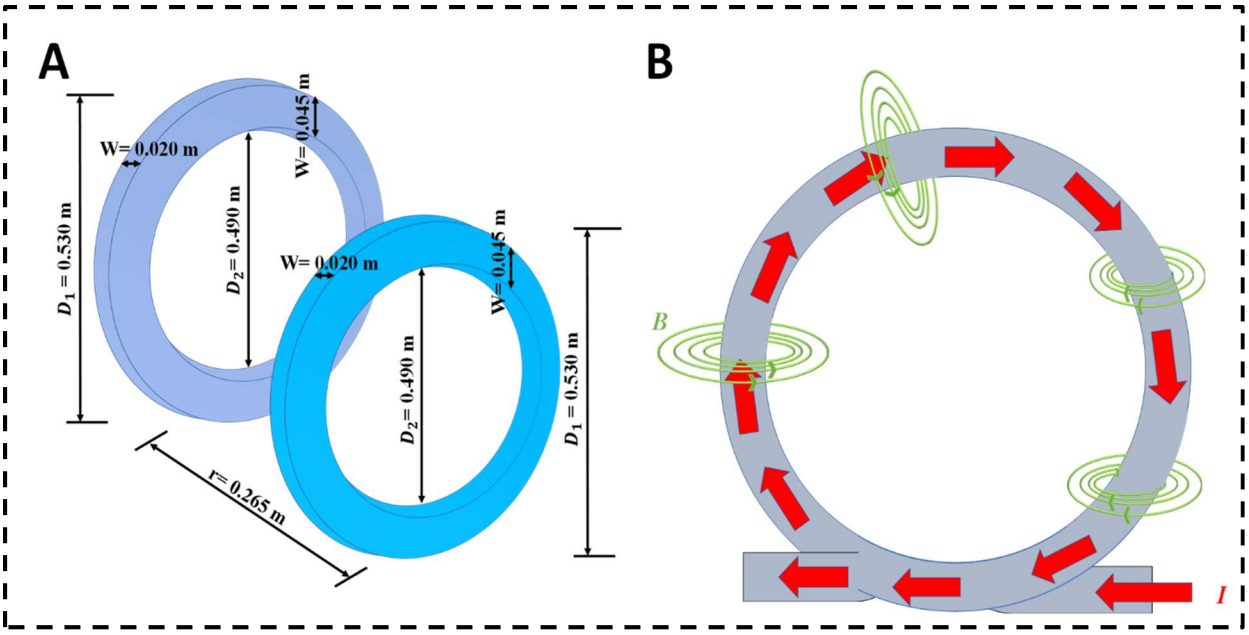

Figure 2.2 Structural configuration of Helmholtz coil system. (A) Schematic of Helmholtz coils, (B) MF orientation due to current flow inside coils. All dimensions are given in meters.

2.2.5.2 Electrical design

The primary considerations in designing an effective Helmholtz coil system are reducing coil impedance and maintaining spatial limitations, field gradient, and field intensity between the coils. In addition, several other factors, i.e., wire gauge, no. of wire turns, and coil circuit configuration, must be considered (Cvetkovic et al., 2006; Cvetkovic and Cosic, 2007; Mahnam et al., 2016; Raganella et al., 1994) as shown in figures 2.3(A-B).

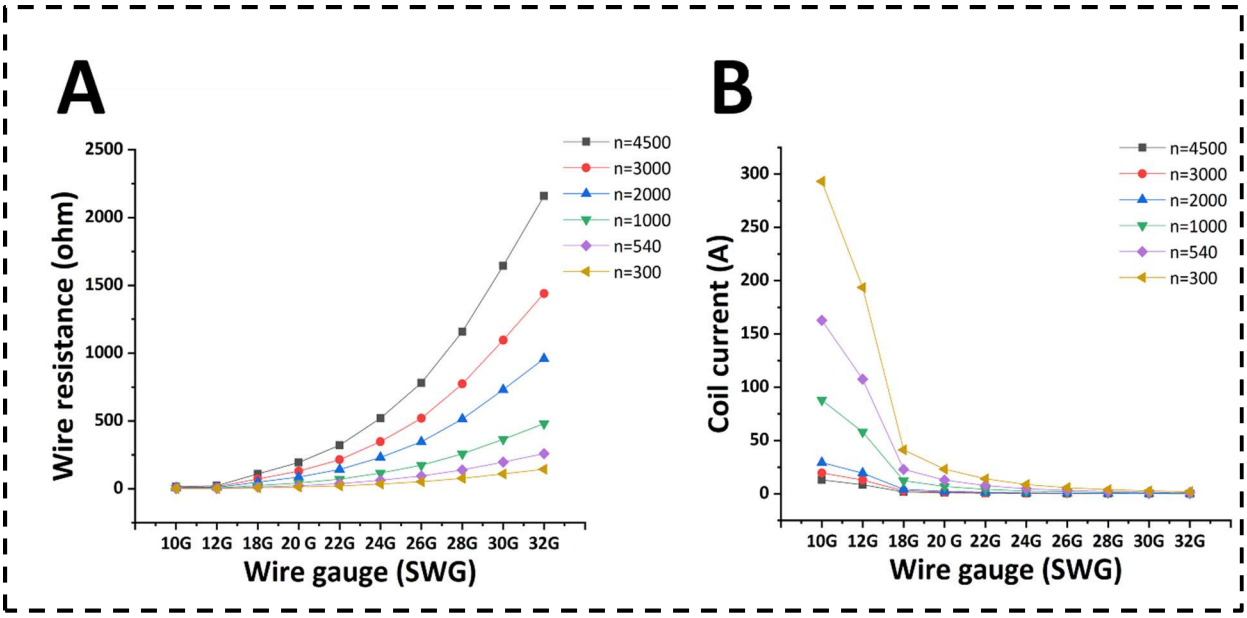

Figure 2.3 Relationship between wire gauge, coil current, and wire resistance. (A) Relationship between wire resistance and wire gauge, (B) Relationship between coil current and wire gauge.

2.2.5.2.1 Spatial limitations

According to Helmholtz coil configuration, we need to maintain the coil separation distance (r) equal to the coil radius (R_c), as shown in equation (2.8). Here, the coil separation distance is equivalent to "$(d_w \times N^{0.5})$" for a square cross-section with number of turns (N), wire diameter (d_w) and thickness of the coil (Salvatore et al., 2012). Then, we must consider the following expression

$$(d_w) \times N^{\frac{1}{2}} < \frac{D}{2} \qquad (2.9)$$

Now, the total wire resistance can be represented by the following expression.

$$R = \rho\left(\frac{L_w}{A}\right) \qquad (2.10)$$

and

$$L_w = \frac{R*\pi\,(d_w)^2}{4\rho} \qquad (2.11)$$

Here,

$D =$ Coil diameter in meters $(M^0L^1T^0)$

$R =$ Resistance of straight wire in Ohm $(\Omega)(M^1L^2T^{-3}A^{-2})$

$d_w =$ Diameter of wire in meters $(M^0L^1T^0)$

$D =$ Coil diameter in meters $(M^0L^1T^0)$

$L_w =$ Length of wire in meters $(M^0L^1T^0)$

$\rho =$ Resistivity of wire in ohm $-$ meter $(\Omega * m)(M^1L^3T^{-3}A^{-2})$

$$l = 2\pi\frac{D}{2}N \qquad (2.12)$$

Therefore,

$$N = \frac{R(d_w)^2}{4\rho D} \qquad (2.13)$$

as d_w increases, $t = d_w \times N^{0.5}$, using equation (2.13), gives

$$t = (d_w)^2\left(\frac{R}{4\rho D}\right)^{\frac{1}{2}} \qquad (2.14)$$

The influence of spatial limitations and the relationship between magnetic flux density (B), wire radius, and cross-sectional area of the wire are depicted in figures (2.4-2.5).

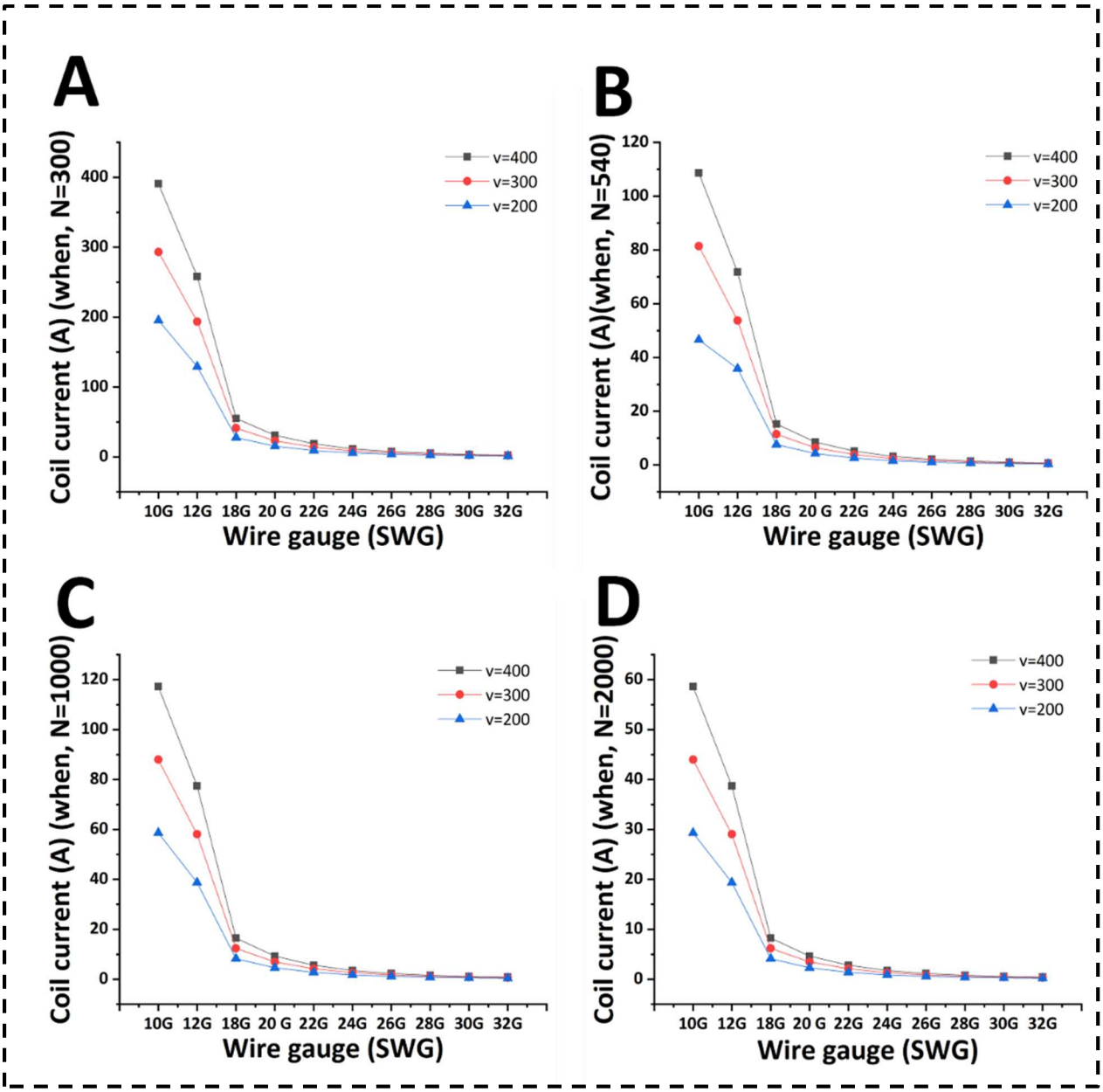

Figure 2.4 Spatial limitations in the development of Helmholtz coils. (A) Relationship between coil current and wire gauge when no. of wire turns (N) is 300 turns/coil, (B) Relationship between coil current and wire gauge when no. of wire turns (N) is 540 turns/coil, (C) Relationship between coil current and wire gauge when no. of wire turns (N) is 1000 turns/coil, (D) Relationship between coil current and wire gauge when no. of wire turns (N) is 2000 turns/coil.

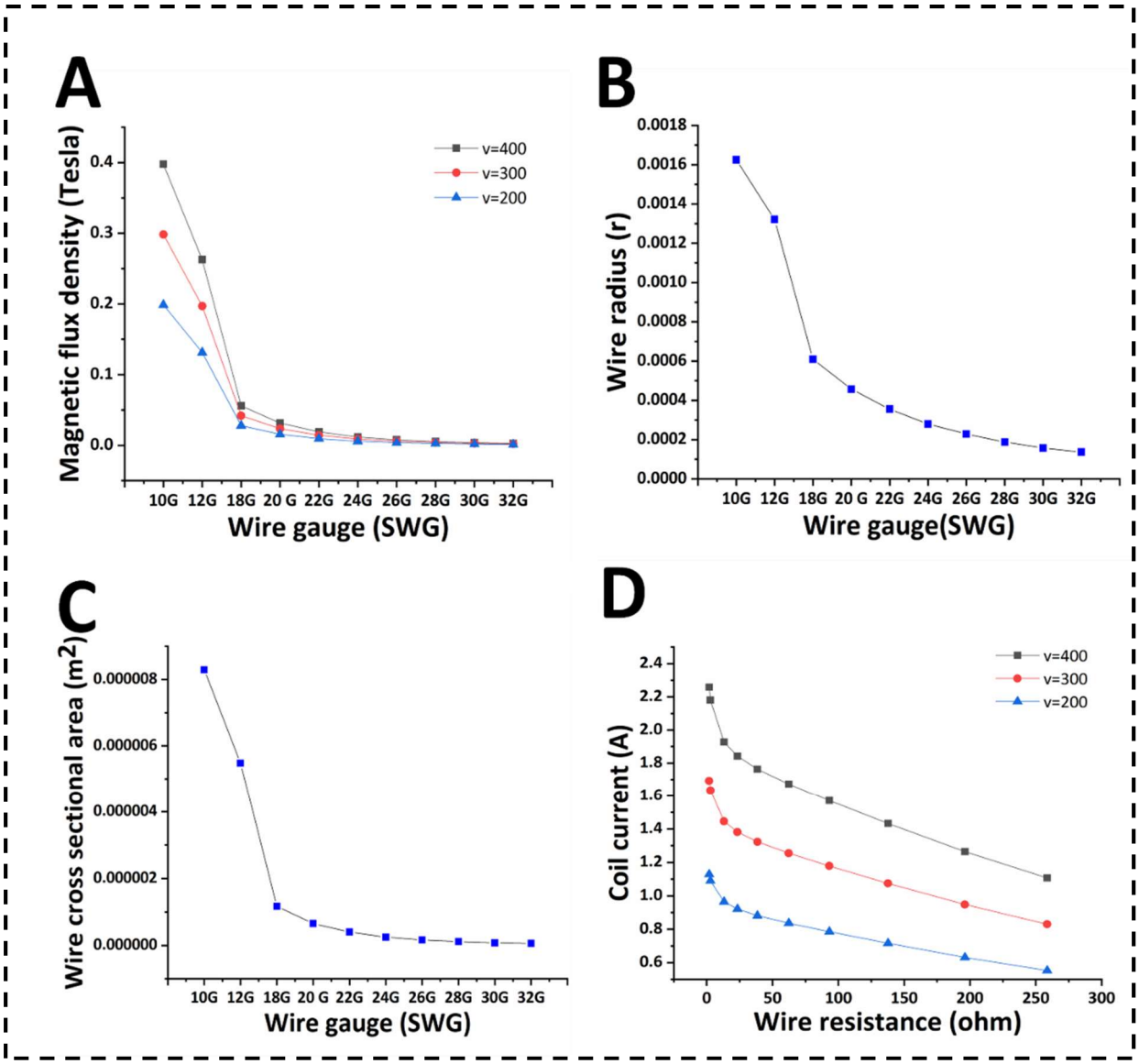

Figure 2.5 Relationship between magnetic flux density, wire radius, cross-sectional area and wire gauge. (A) Relationship between magnetic flux density and wire gauge, (B) Relationship between wire radius and wire gauge, (C) Relationship between cross-sectional area and wire gauge, (D) Relationship between coil current and wire resistance.

2.2.5.2.2 Coil inductance

The following expressions can calculate the self-inductance and loop inductance of the conductor:

$$L_{wire} = 2L_w \left[\ln\left\{ \left(\frac{2L_w}{d_w}\right)\left(1 + \sqrt{1 + \left(\frac{d_w}{2L_w}\right)^2}\right)\right\} - \sqrt{1 + \left(\frac{d_w}{2L_w}\right)^2} + \frac{\mu}{4} + \left(\frac{d_w}{2L_w}\right)\right] \quad (2.15)$$

and

$$L_{loop} = \mu_0 \mu_r \left(\frac{D}{2}\right)\left[\ln\left(\frac{8D}{d_w}\right) - 2\right] \quad (2.16)$$

Here,

L_{wire} = Inductance of straight wire in Henry (H) $(M^1L^2T^{-2}A^{-2})$

d_w = Diameter of wire in meters (m) $(M^0L^1T^0)$

L_w = Length of wire in meters (m) $(M^0L^1T^0)$

D = Coil diameter in meters (m) $(M^0L^1T^0)$

μ = Permeability

μ_0 = Permeability of free space $(4\pi \times 10^{-7}\ H/m)(M^1L^1T^{-2}A^{-2})$

μ_r = Relative permeability

The following expressions can represent the coil inductance, mutual inductance, and coupling factor in Helmholtz coil configuration.

$$L_{coil} = \mu_0 * \mu_r \frac{A*(N)^2}{2*(R_c)} \qquad (2.17)$$

$$M = \sqrt{L_{coil1} * L_{coil2}} \qquad (2.18)$$

and

$$K = \frac{M}{\sqrt{L_{coil1} * L_{coil2}}} \qquad (2.19)$$

Here,

L_{coil} = Inductance of coil in Henry (H)$(\frac{N^2}{R})$ $(M^1L^2T^{-2}A^{-2})$

M = Mutual inductance of coil in Henry (H) $(M^1L^2T^{-2}A^{-2})$

k = Coupling factor between coil

In the Helmholtz coil system, the connection can be a series or parallel circuit depending upon the requirement, i.e., static/pulsed magnetic field. The supply frequency is in ELF range (≈ 50 Hz) under experimental conditions. Hence, the Helmholtz coil shown here is better suited for ELF applications (Anderson, 1999; Bronaugh, 1995; Javor and Anderson, 1998).

The apparent power is the total power available to run any device, but the real power is used for a specific load. Apparent power is a combination of real power and reactive power. Real power is a result of resistive components, and reactive power is a result of capacitive and inductive components, commonly implemented in all circuits. The apparent power (s), real power (P), and reactive power (Q) is represented by the following expressions.

$$S = V * I * e^{j\theta} \quad (2.20)$$

and

$$S = V * I * \{\cos(\theta) + j\sin(\theta)\} \quad (2.21)$$

As shown in equations (2.20) & (2.21), real power (P) and reactive power (Q) can be expressed as

$$P = V * I * \cos(\theta) \quad (2.22)$$

and

$$Q = V * I * j\sin(\theta) \quad (2.23)$$

Here,

$V =$ Voltage in the circuit (Volt) $(M^1L^2T^{-3}A^{-1})$

$I =$ Current in the circuit (Ampere) $(M^0L^0T^0A^1)$

$\theta =$ Angle between voltage and current in the circuit

The Helmholtz coil system's electrical design depends on selection of wire gauge to facilitate ease in the coiling process and limit the wire length or number of wire turns to control the coil's total inductance (Batista et al., 2018), as depicted in figure (2.5). Hence, we selected 20 standard wire gauges (SWG) to support current levels ($\leq 4\,A$) without overheating or losing the insulation capacity of wires. As mentioned in equations (2.7), (2.12), and (2.13), magnetic flux density (B), the wire turns (N), total resistance (R), and length of wire (L_w) is calculated, which is summarized in table 2.1. It is crucial to note that the current, voltage, and power are maximum values in experimental conditions.

Table 2.1 manifests the design framework concerning the fabrication of the device. The coil inductance (L) and mutual inductance (M) are almost the similar according to equations (2.17) & (2.18), and the coupling factor is equal to one, as represented in equation (2.19). Tables (2.2-2.3) represent the electrical parameters obtained on the Helmholtz coil prototype for generating and maintaining the magnetic field.

Table 2.1 Theoretical electrical parameters for Helmholtz coil system.

No. of turns "N"	**Wire length (L_w) (m)**	**Resistance (Ω)**	**Current (A)**	**Voltage (V)**	**Power (W)**
540	898.668	23.3	1.00	75	75
540	898.668	23.3	2.00	132	264
540	898.668	23.3	3.00	189	567

Table 2.2 Electrical parameters obtained on Helmholtz coil prototype.

No. of turns "N"	**Coil outer diameter (D) m**	**Wire diameter (d_w) m**	**Wire inductance (L_{wire}) H**	**Loop inductance (L_{loop}) H**	**Coil inductance (L_{coil}) H**	**Mutual inductance (M) H**	**Coupling factor (k)**

540	0.530	0.0009 14	2.55E +04	4.84E-09	4.53E-07	4.53E-07	1

Table 2.3 Electrical parameters obtained for generation and maintenance of uniform magnetic field.

No. of turns "N"	**Wire length (L_w) m**	**Measured resistance (Ω)**	**Max. current (A)**	**Max. voltage (V)**	**Max power (W)**	**Max magnetic field (mT)**
540	898.668	23.3	1.0	75	75	1.18
540	898.668	23.3	2.0	132	264	2.25
540	898.668	23.3	3.0	189	567	3.19

2.2.6 Computational simulation of MF distribution and intensity

The analysis of spatial MF distribution between monoaxial Helmholtz coil systems for outer diameter ($D_1 = 0.530$ m), inner diameter ($D_2 = 0.490$ m), coil thickness ($t = 0.020$ m), and coil separation distance ($r = 0.265$ m) were analyzed. The current direction in coils is shown in figure 2.2(B). The computational simulation of MF generation showed that magnetic flux density (B) is strongly dependent on number of wires turns (N) and coil separation distance according to equation 2.8. Additionally magnetic flux direction depends on current direction in both coils. Initially, we selected voltage and current values ($V = 75\ volts$ & $I = 1\ A$) and magnetic field (400 μT) and magnetic field intensity is achieved as depicted in figure 2.6 (A). Figure 2.7 (A) shows that flux

density is maximum on coil surface which gradually reduced as we move toward center of coils. Again, we repeated the same process with different voltage and current values ($V = 132\ volts, 189\ volts$ & $I = 2\ A, 3\ A$) and 850 μT and 1.26 mT was achieved respectively as illustrated in figure 2.6 (B-C). Figure 2.7 (B-C) shows the magnetic field overlay for different voltage and current values.

Collectively, we observed that the field generated from both coils becomes additive, and we can maintain uniform MF distribution inside the exposure chamber, as shown in figures (2.6-2.7). Based on the computational simulation study, the dimensions of coils were selected for *in vitro* and *in vivo* experiments.

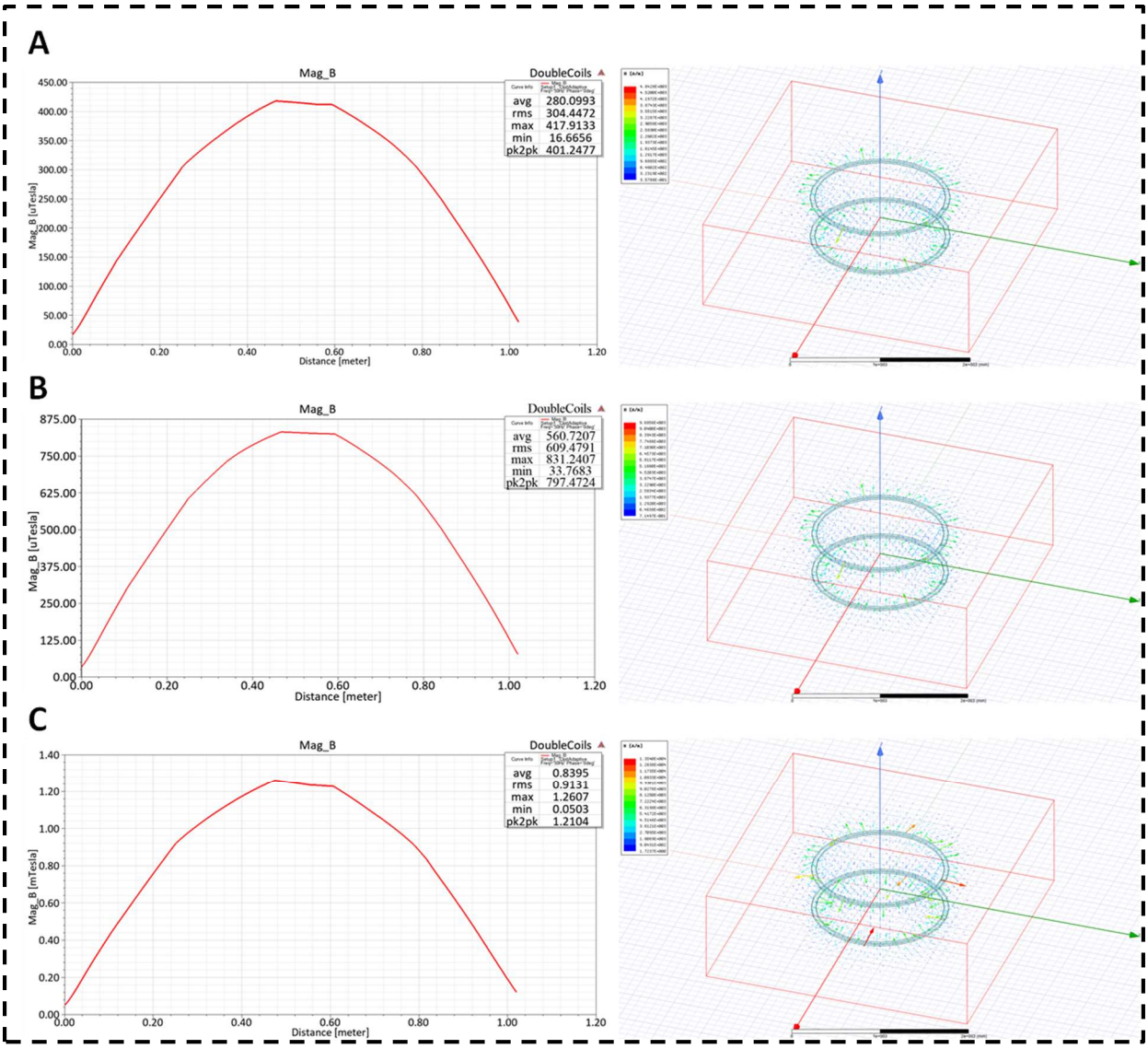

Figure 2.6 Magnetic flux density and MF intensity between Helmholtz coils at different current intensities. (A) Magnetic flux density and MF intensity at y-axis (I = 1 A), (B) Magnetic flux density and MF intensity at y-axis (I = 2 A), (C) Magnetic flux density and MF intensity at y-axis (I = 3 A).

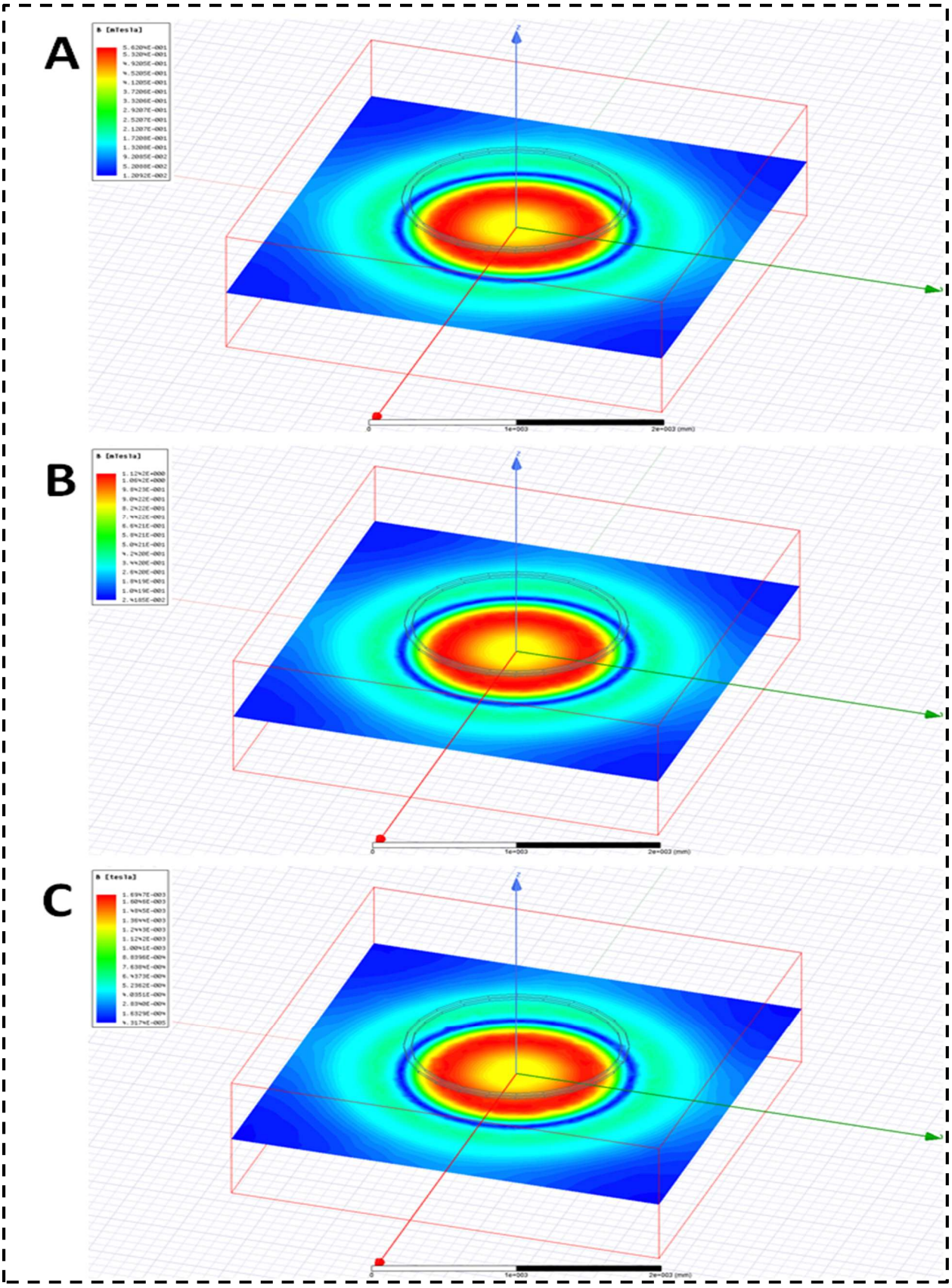
A
B
C

Figure 2.7 MF overlay between Helmholtz coils at different current intensities. (A) MF overlay at yz-plane (I = 1 A), (B) MF overlay at yz-plane (I = 2 A), (C) MF overlay at yz-plane (I = 3 A).

2.2.7 Monoaxial Helmholtz coil system

The schematic diagram of 50 Hz ELF-PEMF exposure system has different components i.e., AC power supply, variable autotransformer (VARIAC), digital voltmeter/ammeter and gaussmeter (MG-3002) as depicted in figure 2.8(A). Figure 2.8(B) illustrates the prototype arrangement of the power supply followed by variable autotransformer, step-up transformer, and digital ammeter/voltmeter connected with Helmholtz coils (parallel configuration) for generation of homogenous MF for *in vivo* and *in vitro* studies. The output of variable autotransformer is fed to the coil system and MF measurement is performed by hand held AC/DC gaussmeter (MG-3002). The coil system also consists of digital ammeter/voltmeter for continuous monitoring of current and voltage levels.

2.2.7.1 Current source

The MF generation inside the Helmholtz coil system is accomplished by maintaining the alternating current flow through the conductor coils. A duty cycle is the fraction of one period in which a signal or system is active, and it is the percentage or ratio of the on-and-off cycle (Brown, 2012). The duty cycle is important because a slight increase/decrease may lead to a significant increase/decrease in the operating peak current and corresponding MF. The supplied current has a frequency (50 Hz) and duty cycle (50%). The Helmholtz coil requires electrical current ($1\ A \leq I \leq 3\ A$), and assuming that the coil has the highest resistance ($23.3\ \Omega/\text{coil}$), powering the coil requires less than 600 Watt for maximum current ($I \leq 3\ A$).

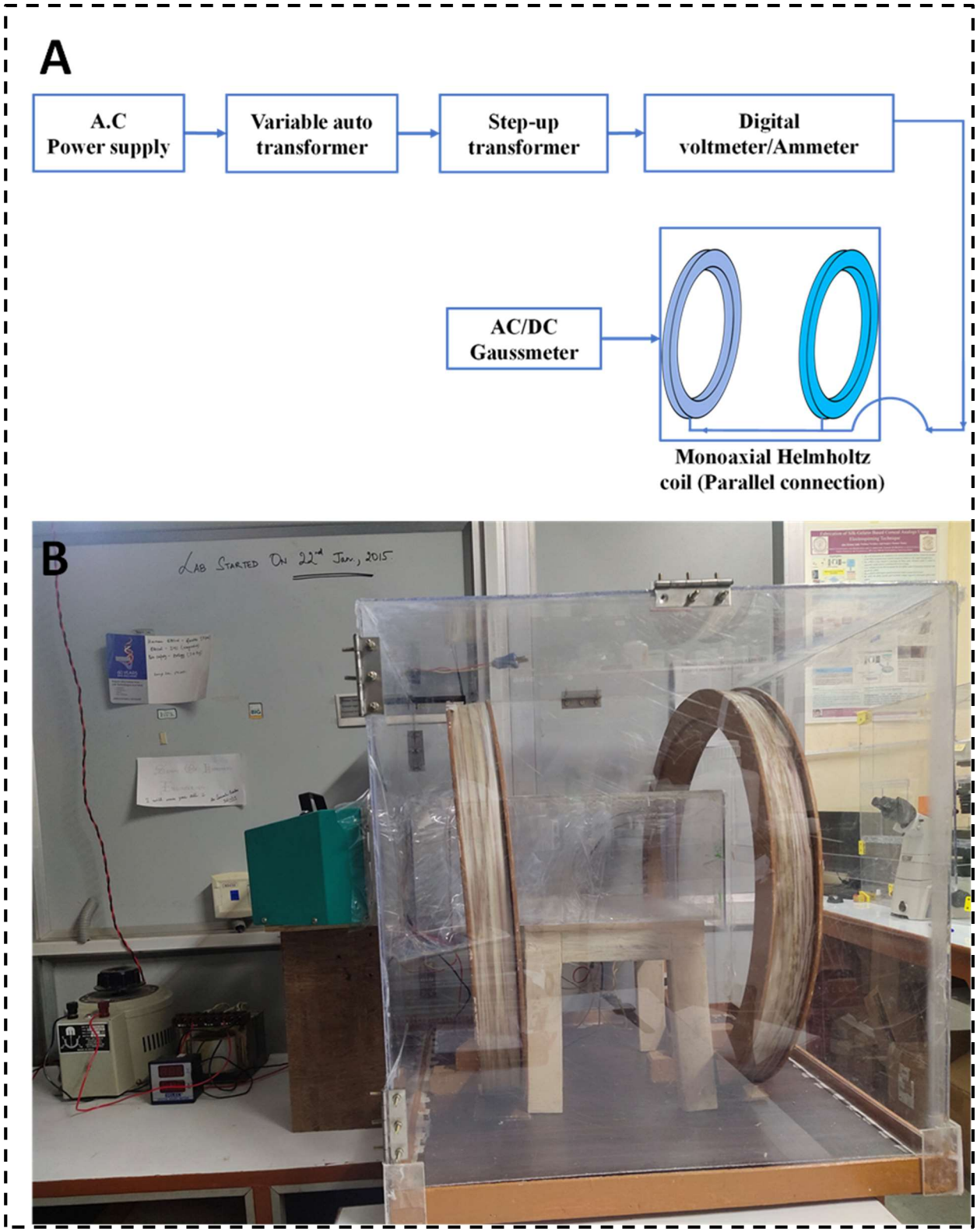

Figure 2.8 Mono-axial Helmholtz coil (parallel configuration) for bioelectromagnetic studies. (A) Schematic representation for 50 Hz ELF-PEMF chambers, (B) Custom-made 50 Hz ELF-PEMF

chamber for *in vivo* and *in vitro* studies.

2.3 Results

2.3.1 Experimental MF analysis

According to computational simulation data, the uniform MF generation system was fabricated and assembled. The MF uniformity was observed with handheld MF sensor (MG3002, Lutron Electronic, Taiwan) with an acrylic sheet arrangement ($l = 20$ cm, $w = 0.5$ cm, $h = 44.5$ cm.) with equidistant holes as depicted in figure 2.9. The sheet was initially placed on $x = 0, y = 0, z = 0$. The supply voltage and current were gradually increased up to $V = 75$ volts & $I = 1$ A thus creating a homogenous field around the center as shown in figure 2.10 (A). The measurements were obtained for the yz-plane at x = 0, and all readings were taken as coordinates at every 2 cm slot mark on the acrylic sheet while keeping $x = 0, y = -5$ to 5, and $z = -7$ to 7 for one set of readings. The above process of homogenous MF generation was also repeated for $V = 132$ & 189 volts & $I = 2$ & 3 A respectively as shown in figures 2.10 (A-C). Tables (2.3-2.4) show the electrical parameters and MF homogeneity data, as represented in figures (2.5 & 2.10) respectively. Table 2.5 shows the temperature variation in coils during the experimental duration. The experimental results with gaussmeter were in good agreement with the computational simulation results.

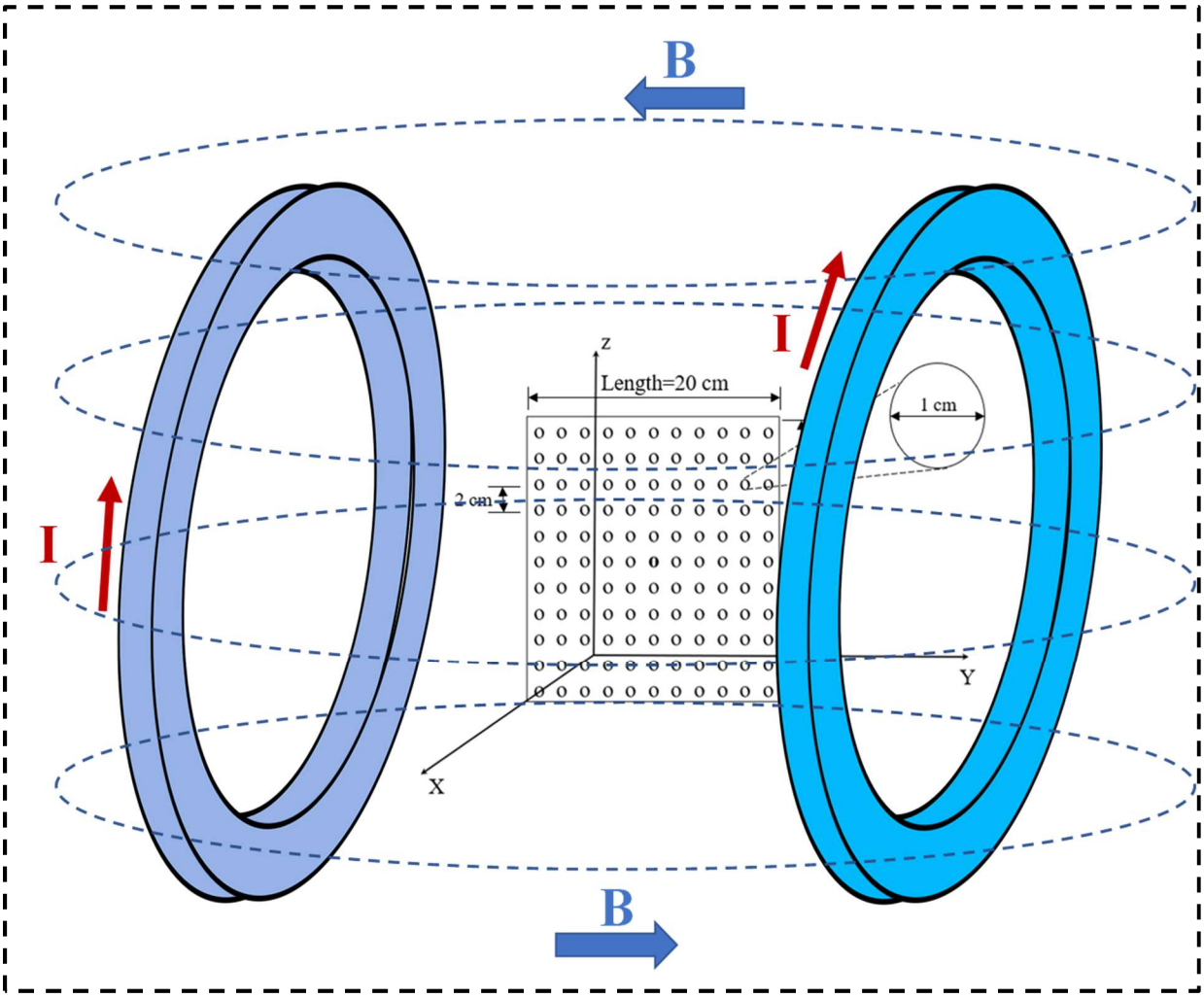

Figure 2.9 Schematic of experimental MF measurement with acrylic sheet arrangement with equidistant holes.

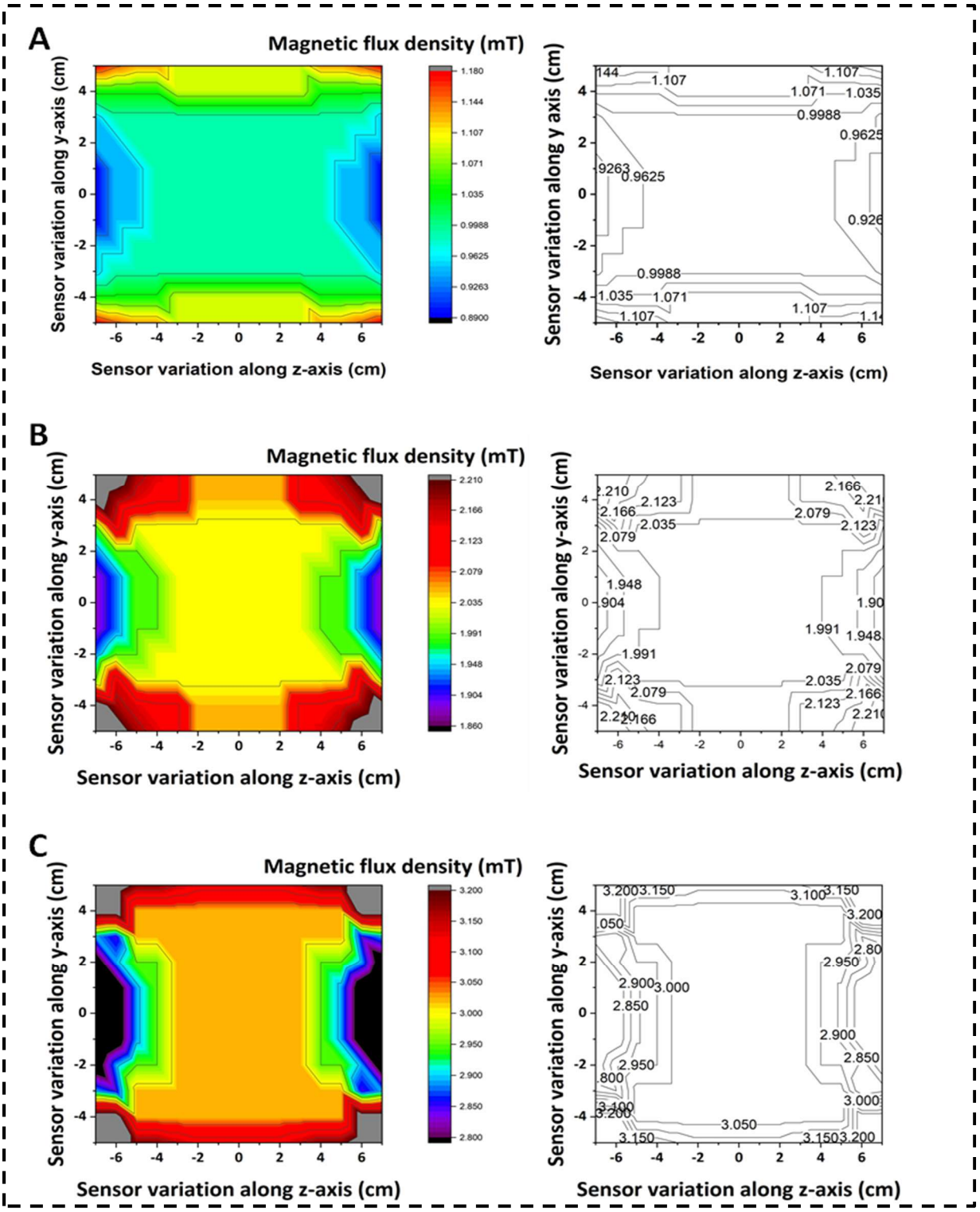

Figure 2.10 50 Hz ELF-PEMF distributions between Helmholtz coils at different loading voltages. (A) Magnetic flux density vs. sensor movement along the z-axis for a voltage and current range ($V = 75$ volts, $I = 1.0$ A), (B) Magnetic flux density vs. sensor movement along the z-axis for a

voltage and current range ($V = 132$ volts, $I = 2.0$ A), (C) Magnetic flux density vs. sensor movement along the z-axis for a voltage and current range ($V = 189$ volts, $I = 3.0$ A).

Table 2.4 Magnetic field homogeneity at the center of the Helmholtz coil system for $I = 1 - 3$ A.

Area (cm^2) (30×35.5)	**Central field (mT)**	**Lowest field (mT)**	**Highest Field (mT)**	**(Field variation) (mT)**
$I = 1$ A	0.99	0.95	1.18	0.23
$I = 2$ A	2.0	1.94	2.25	0.31
$I = 3$ A	3.0	2.85	3.19	0.34

Table 2.5 Temperature variation in coils during the experimental duration.

Current (A)	**Room temperature (T_R)**	**Initial temperature (T_1) ˚C**	**Final temperature (T_2) ˚C**	**Duration of exposure (min.)**
$I = 1$ A	21.8	21.8	22.9	20
$I = 2$ A	21.8	22.9	28.5	20
$I = 3$ A	21.8	28.5	36.5	20

2.4 Discussion

The Helmholtz coil system is fabricated using an 0.5-inch thick plywood circular frame of a circumference ($2\pi r = 1.664$ m), wire length ($\mathrm{L} = 898.668$ m) for coil radius ($R = 0.265$ m) using the copper wires of diameter ($\mathrm{d} = 0.914 \times 10^{-3}$m) for 20 Standard Wire Gauge (SWG) and cross-sectional area ($A = 6.558 \times 10^{-7}$m²) with wire turns ($N = 540$), coil winding was done manually but machine-aided. We have used 20 SWG copper stranded wires for maximizing the coil current due to an increase in cross-sectional area and reduction in coil resistance to generate a homogenous MF without increasing the wire length as per equations (2.7), (2.12) & (2.13). The device's capability to generate a MF (≤ 3 mT) can cancel the earth's MF (≤ 1.2 Gauss) on any axis. The coils are supplied by voltage supply ($75 - 190$ volts), 50 Hz power supply for establishing a uniform MF ($\mathrm{B} = 1 - 3$ mT). No EM wave would emit from coils at this low frequency, so there won't be any EM interference issue. Hence faraday cage is not required in the present setup. The custom-made coils for the experimental setup were multiturn instead of single-turn solid conductor coils to avoid eddy current flows in the coil due to the skin effect and proximity effect. Hence, it can be reasonably assumed that working (AC) resistance is more or less equal to apparent (DC) resistance, and reasonably accurate results can be anticipated. In the present study, we also analyzed temperature variation to determine the temperature at the end of each exposure period. We have designed the incubation chamber with a 0.5 cm thick acrylic sheet having dimensions $\mathrm{length} = 30$ cm, $\mathrm{height} = 17$ cm, $\mathrm{width} = 25$ cm for *in vitro* studies as shown in figure (2.8). The incubation chamber is also equipped with a temperature sensor and controller (tAPMAN 48 7E-1) with distilled water in a petri-dish to maintain temperature (37 ± 2 ˚C) and humidity inside the chamber as necessary requirement for *in vitro* studies. We used a Mextech DT-9 pen-type stainless steel thermometer to observe the temperature variation on coil

surface under standard laboratory conditions, as illustrated in table 2.5.

The MFs is homogenous around the incubation chamber at the coil's center, as depicted in figure (2.10). The current required to generate a homogenous MF inside the coils for current range ($I = 1 - 3$ A) and considering each pair resistance, power ($P \leq 600$ Watt) is required to power the coils for different voltage ranges as shown in table 2.1. Tables 2.2 & 2.3 show the obtained electrical parameters and MF homogeneity data for the total area ($30 \times 35.5\ cm^2$): the field strength at the center, the highest and lowest field strength in the region, respectively. As this magnetic coil system will age, factors such as design, material, maintenance, operational wear and tear will contribute to its failure. The repeated use of this system will cause the operational wear and tear but we can use this system easily up to 5-7 years.

2.5 Conclusion

In this chapter, we have discussed the significant design factors, i.e., wire gauge and spatial limitations, involved in the design of Helmholtz coil system for *in vivo* or *in vitro* bioelectromagnetic studies as reported by various research articles (Lodato et al., 2013; Paksy et al., 2000; Valberg, 1995). We have inscribed all significant factors in design and development along with mathematical expressions of the geometric parameters. The Helmholtz coil configuration was employed to improve the quality of the magnetic field uniformity and reduce the losses at the applied frequency. The primary advantage of the current setup was minimal interference from ferromagnetic materials in the magnetic field environment. Despite using a more straightforward constructive design, the results were better than other coils described in the literature.

2.6 References:

Alvarez, A.F.R., Franco-Mejia, E., Pinedo-Jaramillo, C.R., 2012a. Study and analysis of magnetic field homogeneity of square and circular helmholtz coil pairs: A taylor series approximation, in: Proceedings of the 6th Andean Region International Conference, Andescon. pp. 77–80. https://doi.org/10.1109/Andescon.2012.27

Alvarez, A.F.R., Franco-Mejia, E., Pinedo-Jaramillo, C.R., 2012b. Study and analysis of magnetic field homogeneity of square and circular helmholtz coil pairs: A taylor series approximation. Proc. 6th Andean Reg. Int. Conf. Andescon 2012 0, 77–80. https://doi.org/10.1109/Andescon.2012.27

Anderson, T., 1999. Design of a Helmholtz coil for susceptibility testing using variational calculus and experimental verification. IEEE Int. Symp. Electromagn. Compat. 2, 601–604. https://doi.org/10.1109/ISEMC.1999.810084

Batista, D.S., Granziera, F., Tosin, M.C., de Melo, L.F., 2018. Three-Axial Helmholtz Coil Design and Validation for Aerospace Applications. IEEE Trans. Aerosp. Electron. Syst. 54, 392–403. https://doi.org/10.1109/TAES.2017.2760560

Bronaugh, E.L., 1995. Helmholtz coils for calibration of probes and sensors: limits of magnetic field accuracy and uniformity, in: IEEE International Symposium on Electromagnetic Compatibility. pp. 72–76. https://doi.org/10.1109/ISEMC.1995.523521

Brown, M.C., 2012. Practical switching power supply design. Elsevier.

Caparelli, E.C., Tomasi, D., 2001. An Analytical Calculation of the Magnetic Field Using the Biot Savart Law. Rev. Bras. Ensino Física 23. https://doi.org/10.1590/s0102-47442001000300005

Cvetkovic, D., Cosic, I., 2007. Modelling and design of extremely low frequency uniform magnetic field exposure apparatus for in vivo bioelectromagnetic studies, in: 29th Annual International Conference of the IEEE Engineering in Medicine and Biology Society. pp. 1675–1678. https://doi.org/10.1109/IEMBS.2007.4352630

Cvetkovic, D., Jovanov, E., Cosic, I., 2006. Alterations in human EEG activity caused by extremely low frequency electromagnetic fields, in: International Conference of the IEEE Engineering in Medicine and Biology - Proceedings. pp. 3206–3209. https://doi.org/10.1109/IEMBS.2006.259314

Grant, I.S., Phillips, W.R., 2013. Electromagnetism. John Wiley & Sons.

Javor, E.R., Anderson, T., 1998. Design of a Helmholtz coil for low frequency magnetic field susceptibility testing, in: IEEE International Symposium on Electromagnetic Compatibility. IEEE, pp. 912–917. https://doi.org/10.1109/isemc.1998.750329

Jones, D.S., 2013. The theory of electromagnetism. Elsevier.

Kohli, H., Srivastava, S., Oza, M., Chouhan, S., Verma, S., Bansal, A., Kumar, B., Sharma, S.K., 2022. Design and study of novel tunable ELF-PEMF system for therapeutic applications. IETE J. Res. 68, 2723–2735.

Lodato, R., Merla, C., Pinto, R., Mancini, S., Lopresto, V., Lovisolo, G.A., 2013. Complex magnetic field exposure system for in vitro experiments at intermediate frequencies. Bioelectromagnetics 34, 211–219. https://doi.org/10.1002/bem.21758

Mahnam, A., Yazdanian, H., Mosayebi Samani, M., 2016. Comprehensive study of Howland circuit with non-ideal components to design high performance current pumps. Meas. J. Int. Meas. Confed. https://doi.org/10.1016/j.measurement.2015.12.044

Modi, A., Singh, R., Chavan, V., Kukreja, K., Ghode, S., Manwar, K., Kazi, F., 2016. Hexagonal coil systems for uniform magnetic field generation, in: 2016 IEEE Asia-Pacific Conference on Applied Electromagnetics (APACE). IEEE, pp. 47–51.

Paksy, K., Thuróczy, G., Forgács, Z., Lázár, P., Gáti, I., 2000. Influence of sinusoidal 50-Hz magnetic field on cultured human ovarian granulosa cells. Electromagn. Biol. Med. 19, 91–97.

Raganella, L., Guelfi, M., D'Inzeo, G., 1994. Triaxial exposure system providing static and low-frequency magnetic fields for in vivo and in vitro biological studies. Bioelectrochem. Bioenerg. 35, 121–126. https://doi.org/10.1016/0302-4598(94)87022-5

Ramsden, E., 2011. Hall-effect sensors: theory and application. Elsevier.

Restrepo-álvarez, A.F., Franco-Mejía, E., Cadavid-Ramírez, H., Pinedo-Jaramillo, C.R., 2017. A simple geomagnetic field compensation system for uniform magnetic field applications. Rev. Fac. Ing. Univ. Antioquia 65–71. https://doi.org/10.17533/udea.redin.n83a09

Rubik, B., 2002. The biofield hypothesis: Its biophysical basis and role in medicine. J. Altern. Complement. Med. 8, 703–717.

Salvatore, C., Antonino, L., Francesco, R.F., Alessandro, S., 2012. Accurate design of Helmholtz coils for ELF Bioelectromagnetic interaction by means of Continuous FSO. Int. J. Appl. Electromagn. Mech. 39, 665–669. https://doi.org/10.3233/JAE-2012-1526

Shupak, N.M., Prato, F.S., Thomas, A.W., 2003. Therapeutic uses of pulsed magnetic-field exposure: a review. URSI Radio Sci. Bull. 2003, 9–32.

Valberg, P.A., 1995. Designing EMF experiments: What is required to characterize "exposure"? Bioelectromagnetics 16, 396–401. https://doi.org/10.1002/bem.2250160608

Vallbona, C., Richards, T., 1999. Evolution of magnetic therapy from alternative to traditional medicine. Phys. Med. Rehabil. Clin. N. Am. 10, 729–754.